LEGIBILITY NOTICE

A major purpose of the Technical Information Center is to provide the broadest dissemination possible of information contained in DOE's Research and Development Reports to business, industry, the academic community, and federal, state and local governments.

Although a small portion of this report is not reproducible, it is being made available to expedite the availability of information on the research discussed herein.

Los Alamos National Laboratory is operated by the University of California for the United States Department of Energy under contract W-7405-ENG-36

LA-UR--90-539

DE90 007541

TITLE BOSE CONDENSATE IN SUPERFLUID ^{4}He AND MOMENTUM DISTRIBUTIONS BY DEEP INELASTIC SCATTERING

AUTHOR(S): Richard N. Silver, T-11
Paul E. Sokol*

SUBMITTED TO: Proceedings: Recent Progress in Many-Body Theories II
to be published by Plenum Press

*Dept. of Physics
Pennsylvania State University
University Park, PA 16802

BOSE CONDENSATE IN SUPERFLUID ^{4}He AND MOMENTUM DISTRIBUTIONS BY DEEP INELASTIC SCATTERING

Richard N. Silver

Theoretical Division and Los Alamos Neutron Scattering Center
MS B262 Los Alamos National Laboratory
Los Alamos, New Mexico 87545

Paul E. Sokol

Department of Physics
The Pennsylvania State University
University Park, PA 16802

INTRODUCTION

In 1938 London [1,2] offered an explanation of the observation earlier that year of superfluid behavior in liquid ^{4}He when it is cooled below a critical temperature of 2.17 °K. He argued that the superfluid transition was analogous to the Bose condensation of an (*ideal*) gas of non–interacting atoms obeying the same Bose–Einstein spin–statistics relation as ^{4}He atoms. This relation requires the many–atom wave function to be completely symmetric in the atomic coordinates, resulting in a preference for the atoms to occupy the same single–particle states. For a finite system of atoms the momenta are quantized in spacings proportional to the inverse of the system size. At high temperatures the fraction of atoms occupying any one of the momentum states also scales as the inverse of the size. However, as the temperature is reduced below a critical *Bose condensation temperature* a significant fraction of the atoms, independent of the system size, begins to occupy the zero–momentum state. The *Bose condensate fraction* of an ideal gas approaches one at zero temperature. For ^{4}He, by analogy, at high temperatures in the normal fluid the condensate fraction should be zero, but as temperatures are reduced below the superfluid transition temperature the condensate fraction should rise to a non–zero value. The effect of the strong interactions among the (*non–ideal*) ^{4}He atoms is to deplete the zero temperature condensate fraction from one in an ideal gas to a value much less than one for ^{4}He. While the analogy between superfluidity and Bose condensation is imperfect, the concept of a Bose condensate in

the superfluid phase has survived. A variety of increasingly sophisticated many–body calculations have predicted a condensate fraction of about 10 % at zero temperature in superfluid ^{4}He at SVP. Because of the importance of superfluidity and the related phenomenon of superconductivity to condensed matter physics, this simple prediction has motivated a more than twenty year effort involving up to one hundred scientists to measure the Bose condensate fraction in ^{4}He.

More generally, the goal has been to measure the *momentum distribution* [3], $n(p)$, which is the probability for an atom to occupy a single–particle state of momentum p. The most promising technique has been neutron scattering experiments at up to 100's of meV energies, such that the neutron energy is much larger than the characteristic energies for the collective behavior of the system such as the phonon–roton spectrum. If the energy transferred by the neutron is also much larger than the potential energies between atoms, then (hopefully!) the *impulse approximation* (IA) may be invoked in which the scattering from the many–atom system is described as the sum of independent single–atom scatterings. This predicts a simple relation between the momentum distribution and the measured scattering cross section. Analogous experiments are of interest in all sub–fields of physics, because the momentum distribution is an experimentally accessible characterization of the many–particle wave function. This includes x–ray Compton scattering at 10's of KeV energies to measure electron momentum distributions, quasi–elastic electron scattering from nuclei at GeV energies to measure nucleon momentum distributions, and electron scattering from nucleons at 100's of GeV energies to measure quark momentum distributions. Such experiments we term *deep inelastic scattering*. Compton scattering experiments for electronic momentum distributions have been very successful. However, experiments on atomic momentum distributions of interest in condensed matter physics, and on nucleon momentum distributions of interest in nuclear physics, have been plagued by uncertainties about the validity of the impulse approximation for the values of energy and momentum transfer which can be realistically achieved.

Thus, there are several reasons for the high interest in the recent experimental and theoretical progress in understanding deep inelastic neutron scattering from liquid ^{4}He: it tests the fundamental London hypothesis of a connection between superfluidity and Bose condensation; it provides a quantitative test of *ab–initio* calculational methods for all systems with strong correlations which are the focus of current quantum many–body research; and it establishes the range of validity of deep inelastic scattering as a method for measuring momentum distributions. In the following sections we introduce the concepts of impulse approximation in more detail, we describe recent progress in the theory for final state corrections to the impulse approximation, we present quantitative predictions for neutron scattering experiments, we compare with recent high energy pulsed neutron source experiments on liquid ^{4}He by P. Sokol and colleagues as well as other attempts to extract the Bose condensate fraction from the neutron scattering data, and we discuss the implications of this progress for future momentum distribution experiments in other systems such as liquid ^{3}He and quasi–elastic electron nucleus scattering.

THE IMPULSE APPROXIMATION AND THE BOSE CONDENSATE

For the sake of clarity, in this section we explicitly consider only neutron scattering from many–atom systems, although the concepts we shall discuss are common to many other subfields of physics.

In the impulse approximation, the neutron scattering law may be written as the sum of collisions from individual atoms which have a probability of having an initial momentum, p, given

by the momentum distribution, $n(p)$. The energy and momentum transferred by the neutron are assumed to be high enough that the collective dynamics and interactions among He atoms only show up in initial state momentum distribution, $n(p)$, and not in the final state. Then, the scattering law may be written:

$$S(Q,\omega) = S_{IA}(Q,\omega) = \frac{1}{\rho}\int \frac{d^3\vec{p}_i}{(2\pi\hbar)^3}\, n(p_i)\, \delta\left(\hbar\omega - E(p_f) + E(p_i)\right) \quad . \qquad (1)$$

Here, $\vec{p}_i$ is the initial momentum of an atom, $\vec{p}_f = \vec{p}_i + \hbar\vec{Q}$ is the final momentum of the recoiling atom after the neutron has transferred momentum $\hbar Q$ and energy $\hbar\omega$, $E(p) = \hbar^2 p^2/2M$ is the kinetic energy, and ρ is the atomic density. The delta function expresses the energy conservation of the scattering process. $S(Q,\omega)$ is normalized so that the integral of it over $\hbar\omega$ equals one. Equation (1) provides the sought for simple relation between the momentum distribution and the scattering law. The impulse approximation predicts that the scattering law peaks at the recoil energy from a particle at rest, $\hbar\omega = \hbar^2 Q^2/2M$. The width of the peak is $\hbar Q \Delta p/M$, where Δp is the width of the momentum distribution, $n(p)$. An experimental test to establish that deep inelastic scattering conditions, but (as we shall dicuss) not necessarily impulse approximation conditions, have been reached is the observation of this peak position varying as Q^2 and peak width varying as Q.

In 1966 Hohenberg and Platzman [4] suggested that the Bose condensate fraction in ^{4}He could be measured by high momentum transfer neutron scattering experiments. For an isotropic system in the presence of a Bose condensate, the momentum distribution may be written

$$n(\vec{p}) = n_o\rho(2\pi\hbar)^3\delta^{(3)}(\vec{p}) + n^*(p) \quad , \qquad (2)$$

where n_o is the Bose condensate fraction, and $n^*(p)$ is a smooth function. Combining Eqs. (1) and (2) yields

$$S_{IA}(Q,\omega) = n_o\delta\left(\hbar\omega - \hbar^2Q^2/2M\right) + S^*_{IA}(Q,\omega) \quad , \qquad (3)$$

where $S_{IA}{}^*(Q,\omega)$ is the contribution to the scattering law from $n^*(p)$. Thus, in the impulse approximation the scattering law is expected to have a sharp delta function peak with weight n_o centered at the recoil energy, which sits atop a broader peak due to the smooth part of the momentum distribution. The central goal of most deep inelastic neutron scattering experiments on liquid ^{4}He has been the observation of this sharp peak in the superfluid at temperatures less than the superfluid transition temperature, $T_\lambda = 2.17$ °K, and the absence of such a peak in the normal fluid at higher temperatures.

It is common to rewrite the scattering law as a *Compton profile*, after analogous x-ray scattering experiments on electron momentum distributions carried out by A. H. Compton and J. W. M. DuMond in the 1920's. For neutron scattering, it is given by

$$J(Y,Q) = \frac{QS(Q,\omega)}{M} \quad , \qquad (4)$$

where

$$Y = \frac{M}{Q}\left(\frac{\omega}{\hbar} - \frac{Q^2}{2M}\right) \quad . \qquad (5)$$

Specializing to the impulse approximation, one obtains

$$J_{IA}(Y) = n_o \delta(Y) + \frac{1}{4\pi^2\hbar^2 Q}\int_{|Y|}^{\infty} dp\ p\ n^*(p) \quad . \qquad (6)$$

Energy conservation in Eq. (1) requires Y to equal the longitudinal wave vector of the atom, or the component of initial momentum which is parallel to the momentum transfer. In the impulse approximation, the Compton profile is centered at and symmetric about $Y = 0$. It is also independent of Q, which is termed *Y–scaling*. This is equivalent to the earlier statement that the peak in $S(Q,\omega)$ has a position varying linearly in Q^2 and a width varying linearly in Q. Figure 1 [6] shows measured Compton profiles for superfluid ^{4}He at Q's of 7, 12 [7] , and 24 A^{-1} [8]. Although the data are instrument broadened wtih a full–width–half–maximum (FWHM) of 0.6 A^{-1}, the fact that these curves for different Q's approximately lie on top of one another is strong evidence for Y–scaling, especially at higher Q's. However, Y–scaling is a necessary, but not a sufficient condition, for the validity of the impulse approximation. G. West [5] was the first to point out that Y–scaling can be true even if the impulse approximation is false. In a following section on final state effects we present an explicit counterexample to the hypothesis that the observation of Y–scaling confirms the impulse approximation.

Quantitative predictions for deep inelastic experiments on ^{4}He can be obtained from the impulse approximation by inputing theoretical momentum distributions, $n(p)$. The solid line in Fig. 2 shows momentum distributions calculated by Greens' Function Monte Carlo (GFMC) [9] at $T = 0$ °K, which predicts an n_o of 9.24 %. The dashed line shows the momentum distribution calculated by Path Integral Monte Carlo (PIMC) [10] at $T = 3.3$ °K, in which n_o is predicted to be zero. Figure 3 shows the corresponding predictions for Compton profiles. The solid line is the GFMC–IA prediction for the superfluid, which has a delta function peak at $Y = 0$ of weight n_o. The dashed line is the PIMC–IA prediction for the normal fluid, which is a smooth function.

The experimental data, such as Fig. 1, show a sharpening around $Y = 0$ as the temperature is reduced into the superfluid. However, there is no direct evidence for a sharp delta function peak in the superfluid at any Q. The issue has been how to infer the value of n_o from the limited data available which inevitably include instrumental broadening, statistical and background uncertainties, and corrections to the impulse approximation at the finite values of Q's which can be achieved. There have been many reports [11] of determinations of n_o, which have involved a succession of improvements in understanding spectrometers, improvements in the data analysis procedure, and increases in the values of Q to better approach the conditions for the validity of the impulse approximation.

The most extensive data analysis of reactor experiments was carried out in 1982 [12] for data in the range 4 $A^{-1} < Q < 7$ A^{-1}. At lower Q's (< 3 A^{-1}) the neutron scattering law is dominated by the collective behavior such as the phonon and roton spectrum and at higher Q's the neutron flux from reactors becomes prohibitively small for high resolution experiments. These data begin to approach the impulse approximation predictions, i.e. the peaks are centered at the recoil energy of a free particle and the widths are proportional to Q. However, there are signifi-

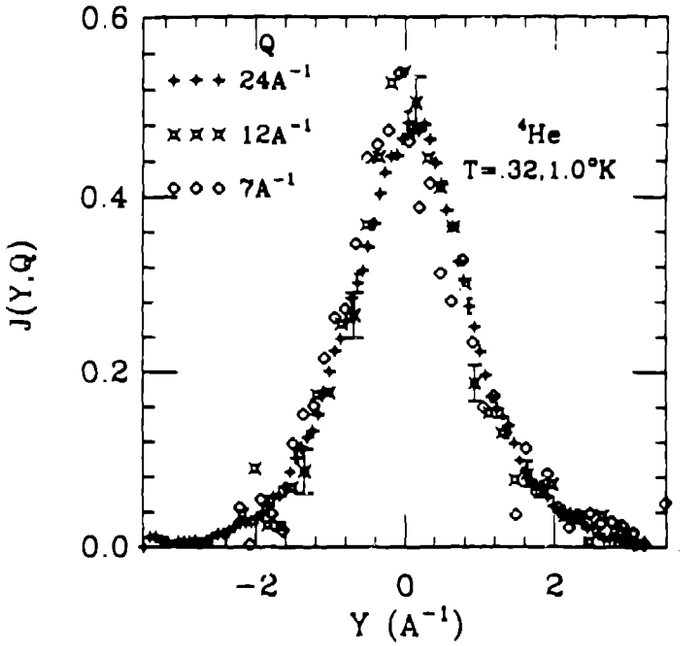

Fig. 1 Inelastic neutron scattering from liquid ^{4}He at momentum transfers of 7 A^{-1}, 12 A^{-1} (at T = 1.0 °K) and 24 A^{-1} (at T = 0.35 °K). The results, plotted as $J(Y)$, all fall on approximately the same curve, illustrating the Y–scaling behavior. The instrumental resolution is about 0.6 A^{-1}.

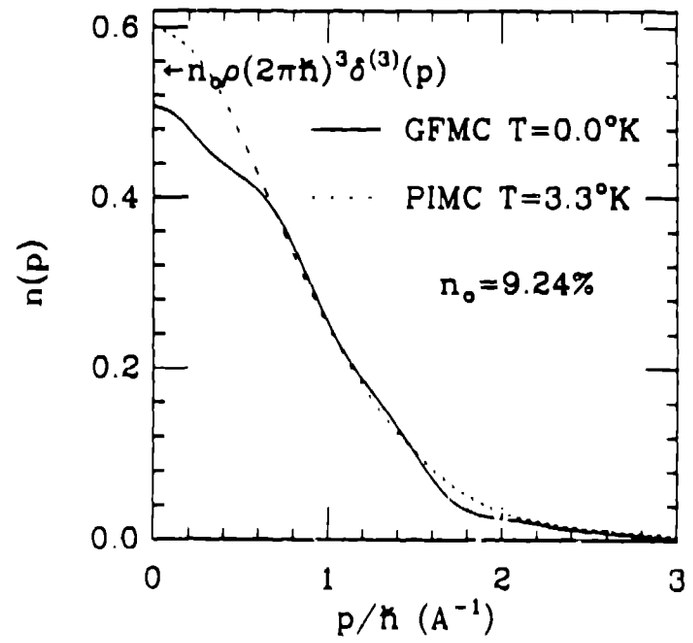

Fig. 2 Theoretical momentum distributions for liquid ^{4}He. The solid line is the Greens' Function Monte Carlo (GFMC) prediction for the superfluid at T = 0 °K, which has a delta function at p = 0 with a 9.2 % Bose condensate fraction. The dashed line is the Path Integral Monte Carlo (PIMC) prediction for the normal fluid at T = 3.33 °K.

cant deviations from the impulse approximation in the form of asymmetry of the peak shape, as shown in the $Q = 7$ A^{-1} data in Fig. 1, and oscillations [13] of the peak width and center with Q. To correct for these deviations, which can be quite significant at lower Q's, the data have been symmetrized about $Y = 0$ and averaged over several Q's. This gives a resultant scattering which is consistent with the basic predictions of the impulse approximation (peaks that are symmetric and centered at the recoil energy) and where the effects of the corrections to the impulse approximation are minimized. The resultant data is then converted from $S(Q, \omega)$ to $n(p)$, which involves a differentiation and a division by p according to Eq. (6).

Attempts to directly compare the experimental momentum distribution, obtained using the procedure above, with theoretical predictions always exhibited significant disagreement. Thus, attention turned to other methods to extract information on the momentum distributions and, especially, the condensate fraction, n_o. The most popular procedure has been modeling of the momentum distribution with n_o as an adjustable parameter.

The model used for the momentum distribution in the superfluid will strongly influence the value of n_o inferred. In fact, several previous studies have inferred a vanishingly small value for the condensate based on a particular model. In the 1982 analysis, only the momentum distribution at small values of p was needed. The model for the uncondensed component of the momentum distribution (i.e. everything but the condensate itself) was:

$$n^*(p) = n_o\left[a/p^2 + b/p\right]\ \theta(p_c - p) + (1 - n_o)\ n(p, T > T_\lambda) \quad . \qquad (7)$$

The first term in this model represents singular behavior that is induced in $n^*(p)$ by the appearance of the condensate [14]. This is due to the coupling of long wavelength phonons to fluctuations in the condensate. The second term simply represents a scaled down version of the normal liquid behavior. The $n(p, T > T_\lambda)$ is fixed by measurements at high temperature where n_o is zero. Based on this model, the 1982 analysis (and subsequent analysis using the same procedure) extracted values of n_o around 10 %, in surprisingly good agreement with theory.

Unfortunately, this apparent agreement between theory and experiment was fortuitous. The small–p singular behavior above, which played a very important role in the 1982 analysis, was the result of an incorrect combination of the small–p and large–p limiting behaviors. Griffin pointed out this error [15]. Using a more correct form for the small–p singular behavior, he obtained values of n_o of 4–5 %, about half the theoretical predictions. More recently, Sokol, Silver and Clark [3] have pointed out that information on the small–p singular behavior is extremely difficult to obtain by deep inelastic neutron scattering measurements, a point to which we will return later.

FINAL STATE EFFECTS

What has been left out of all of the data analysis procedures discussed above has been a detailed understanding of the corrections to the impulse approximation, to which we now turn. These were first addressed in the original paper of Hohenberg and Platzman [4]. The additional physical effect which must be included is the scattering of the recoiling atom from neighboring atoms in the condensed phase, resulting in collisional lifetime broadening. A finite collisional lifetime, τ, results in an uncertainty, $\hbar/\tau$, of the energy of the final state of the He atom after being struck by a neutron, and so this broadening is termed *final state effects* (FSE). This can be important for He even at high Q's, because the potential energy between He atoms is steeply re-

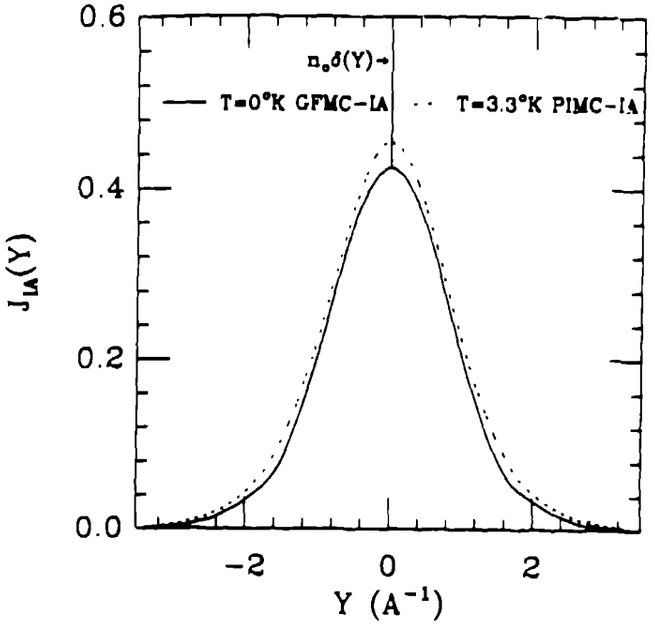

Fig. 3 Compton profiles for ^{4}He calculated in the impulse approximation, $J_{IA}(Y)$. The solid line is the GFMC prediction for the superfluid at $T = 0$ °K, which has a delta function at $Y = 0$ with weight equal to the Bose condensate fraction, n_0. The dashed line is the PIMC prediction for the normal fluid at $T = 3.33$ °K.

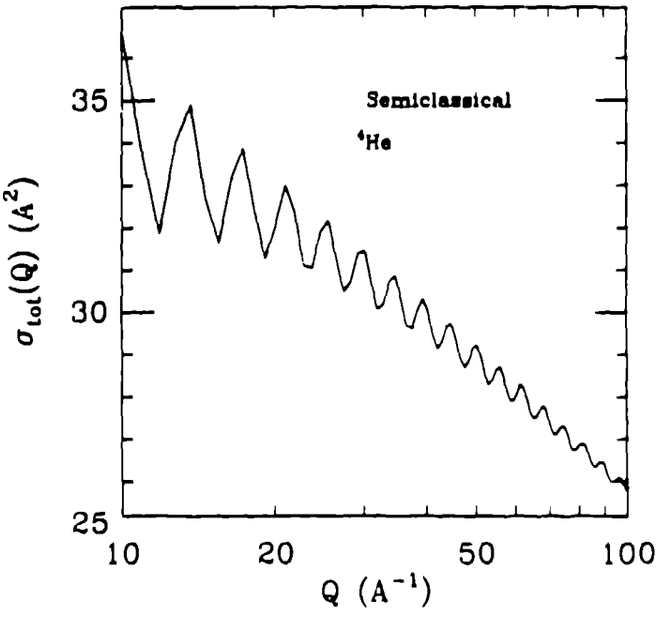

Fig. 4 Semiclassical ^{4}He–^{4}He total cross section for momentum, $\hbar Q$.

pulsive at short distances and never negligible compared to the kinetic energy of the recoiling atom, $\hbar^2 Q^2/2M$.

We now describe this in a fashion which, while not following the original derivation of Hohenberg and Platzman, will naturally lead to our current understanding of final state effects. Assuming that $|\vec{p}_i| \ll \hbar Q$, the rate at which the recoiling atom scatters from neighboring atoms is given by

$$\frac{1}{\tau} = \rho\, \sigma_{tot}(Q)\, \frac{\hbar Q}{M} \quad , \qquad (8)$$

where $\sigma_{tot}(Q)$ is the He–He total scattering cross section for incident momentum $\hbar Q$. The resulting uncertainty in the energy of the recoiling atom is expressed by adding to $E(p_f)$ in Eq. (1) a self energy $\Sigma = -i\hbar/2\tau$. We rewrite the energy conservation delta function in Eq. (1) in terms of its integral representation. Then, the effect of collisions is to transform it as follows:

$$\delta(\Delta E) = \frac{1}{2\pi\hbar}\int_{-\infty}^{\infty} dt\, \exp\left(\frac{it\Delta E}{\hbar}\right) \quad \underset{FSE}{\Rightarrow} \quad \frac{1}{2\pi\hbar}\int_{-\infty}^{\infty} dt\, \exp\left(\frac{it\Delta E - |t|\Sigma}{\hbar}\right) \quad , \qquad (9)$$

where $\Delta E = \hbar\omega - E(p_f) + E(p_i)$ and t can be interpreted as the time after the neutron collision. Then by straightforward manipulations the Compton profile becomes

$$J(Y,Q) = \int_{-\infty}^{\infty} dY'\; R_{FS}(Y-Y',Q)\; J_{IA}(Y') \quad . \qquad (10)$$

The broadening function due to final state effects is given by a Lorentzian form,

$$R_{FS}(Y,Q) = \frac{1}{\pi}\frac{\Gamma}{Y^2+\Gamma^2} \quad , \qquad (11)$$

where $\Gamma = \rho\sigma_{tot}(Q)/2$ is the collision rate per unit distance traveled by the recoiling atom.

Let us first consider those properties of this theory which we believe remain correct in the more modern theories. First, the full–width–half–maximum (FWHM) of the broadening is given by

$$\Delta Y_{FWHM} = \rho\sigma_{tot}(Q) \quad . \qquad (12)$$

(Actually, the original prediction of Hohenberg and Platzman was a factor of two larger than this, and the parameter Y had not yet been suggested as a natural variable for the problem.) In the limit that the He–He potential at short distances can be approximated by a hard sphere, $\sigma_{tot}(Q)$ is independent of Q and equals $2\pi r_o^2$. Here r_o is the hard sphere radius and the factor of 2 is due to forward diffractive scattering. In this limit, the broadening is independent of Q and the Compton profile would satisfy Y–scaling even though the impulse approximation would be invalid. Also, the collision rate per unit distance traveled by the recoiling atom would be $\rho\pi r_o^2$, which is the value given by classical mechanics. In reality, the He–He potential is steeply repulsive, but not hard sphere, at short distances resulting in a $\sigma_{tot}(Q)$ which decreases approximately logarithmically with increasing Q, as shown in Fig. 4. The small *glory oscillations* with Q are a quantum mechanical forward–backward scattering interference effect due to Bose statistics [16]. Then the final state broadening would decrease only logarithmically with increasing Q, resulting in a

However, sum rule arguments show that the Lorentzian lineshape predicted by this theory cannot possibly be correct. The second moment sum rule on the neutron scattering law can be rewritten in terms of the Compton profile as

$$\int_{-\infty}^{\infty} J(Y,Q)\ Y^2\ dY = \frac{2M}{3}\ <K.E.> + O(Q^{-2}) \quad . \qquad (13)$$

The impulse approximation satifies Eq. (13) without the $O(Q^{-2})$ term. If the final state broadening takes the convolution form in Eq. (10), then one must conclude

$$\int_{-\infty}^{\infty} R_{FS}(Y)\ Y^2\ dY = O(Q^{-2}) \quad . \qquad (14)$$

That is, final state effects cannot alter the second moment of the Compton profile from the impulse approximation value in the high Q limit. However, the Lorentzian prediction, Eq. (11), has an infinite second moment. Evidently, final state effects if they exist must be much smaller than given by Eq. (11).

Gersch and Rodriguez [17,18] were the first to address this problem in 1973. They showed how the second moment sum rule could be satisfied with a non–Lorentzian lineshape for the final state broadening. They identified the physical origin of a non–Lorentzian shape as due to a dependence of the He–He scattering rate on the distance traveled by the recoiling atom. This distance dependence was due to the real space correlations which exist among atoms in liquid He. As we shall show, they calculated a final state broadening in qualitative agreement with current neutron scattering measurements. Unfortunately, this work was ahead of its time and did not receive the attention it deserved. One possible source of difficulty was that the derivation used a many–body theory involving time ordered cumulant expansions which were unfamiliar and have not been further developed. Another is that the numerical predictions were buried in an experimental paper which incorrectly obtained a 2 % Bose condensate fraction. Also many of the inputs to the calculation were not yet available and had to be severely approximated, such as approximating the radial distribution function $g(r)$ by a step function.

Since then there have been more than twenty papers on the theory for final state effects in He, and there has been a comparable level of inconclusive activity on the analogous problem in quasielastic electron nucleus scattering in nuclear physics. Many theories continued to obtain quasi–Lorentzian lineshapes which decreased as $O(\ln Q)$ with increasing Q, while other popular theories claimed that the leading correction to the impulse approximation was asymmetric in Y and decreased as $O(Q^{-1})$. Following the Hohenberg Platzman theory several experimental papers [7,19] at low Q ($< 12\ A^{-1}$) have identified apparent oscillations in Q of the width of $J(Y,Q)$ with the glory oscillations in $\sigma_{tot}(Q)$. However, the widths observed are much narrower than the Hohenberg Platzman theory [20]. The premature claims to have observed a 10 % Bose condensate in superfluid ^{4}He in apparent agreement with many–body theory may have contributed to a complacency in the scientific community, i.e. there was a false sense that final state effects were unimportant and the quest to measure the Bose condensate fraction had been achieved [12]. The popular view of the subject up to 1987 has been reviewed by Svensson and Glyde and by Sears

and Svensson [11]. In reality, a distinct delta–function peak in the scattering law had never been directly observed, and the most credible values of the Bose condensate fraction obtained by ignoring final state effects were 4–5 % [15] in serious disagreement with many–body theory.

In 1988 Silver [21,22] published an independent derivation of final state effects which confirmed and built on the original work of Gersch and Rodriguez. We first present a heuristic derivation of the main results of this theory following our derivation of the Hohenberg & Platzman Lorentzian broadening theory presented earlier. There are two elements of new physics: first, the collision rate depends on recoil distance because of correlations in the positions of atoms in the condensed phase; and second, at high Q the De Broglie wavelength of the recoiling atom is short compared to interatomic distances so that a semiclassical description of motion of the recoiling atom is adequate. The distance along the classical trajectory is given by $x = \hbar Qt/M$ where, again, t is the time after the neutron collision. The probability density of finding two atoms a distance x apart is given by $\rho\, g(x)$, where $g(r)$ is the radial distribution function of the liquid. The collision rate at distance x is given by

$$\frac{1}{\tau(x)} = \rho g(x)\sigma_{tot}(Q)\frac{\hbar Q}{M} \quad . \qquad (15)$$

The self energy consequently depends on recoil distance, $\Sigma(x) = -i\hbar/2\tau(x)$.

This essential physics is illustrated in Fig. 5, which shows the He–He potential and the radial distribution distribution function for liquid ^{4}He. The potential is steeply repulsive at short distances and has a weak Van der Waals attraction at larger distances. The radial distribution function shows that the atoms in the condensed phase sit in the attractive part of the potential well far from the steeply repulsive core of the potential. After being struck by a neutron, the recoiling atom must travel for some distance before it begins to collide with the steeply repulsive cores of the potentials from neighboring atoms. Therefore, $1/\tau(x)$ is zero for small x and approaches the value given by Eq. (8) only at large x. So the final state broadening should be much smaller than the Lorentzian broadening prediction.

Then the energy conservation delta function in Eq. (1) becomes

$$\delta(\Delta E) = \frac{1}{2\pi\hbar}\int_{-\infty}^{\infty} dt\, \exp\left(\frac{it\Delta E - it|\Sigma(|t|\hbar Q/M)}{\hbar}\right) \quad . \qquad (16)$$

The final state broadening retains the convolution form, Eq. (10), but now

$$R_{FS}(Y,Q) = \frac{1}{2\pi}\int_{-\infty}^{\infty} dx\, \exp\left[iYx - |x|g(|x|)\Gamma\right] \quad ; \quad \Gamma = \frac{\rho\sigma_{tot}(Q)}{2} \quad . \qquad (17)$$

Let us examine the properties of this final state broadening function. It reduces to the Lorentzian broadening result, Eq. (11), in the limit of a structureless fluid, $g(r) \to 1.0$. The FWHM continues to be approximately given by Eq. (12). Again, a Y–scaling correction to the impulse approximation is obtained in the limit of a hard sphere potential. However, the lineshape is non–Lorentzian and negative at large $|Y|$, and it satisfies the second moment sum rule because $g(0) = 0.0$ in He.

Y–scaling now acquires a geometrical interpretation in the limit of hard sphere interactions between He atoms. *Y* loses its impulse approximation interpretation as the component of initial momentum parallel to the momentum transfer. Instead, *Y* becomes the canonically conjugate variable to the distance, *x*, along the classical trajectory of the recoiling atom. The final state broadening function is the Fourier transform of the probability of no collisions as a function of recoil distance. In the hard sphere limit, the final state effects depend only on the relative positions and sizes of atoms, so that the (potentially 10^{23}) extra variables in the problem drop out. For real potentials, *Y*–scaling is obtained to the extent that $\sigma_{tot}(Q)$ varies slowly with Q.

A formal derivation of a somewhat more correct result has been discussed in detail elsewhere [21,22], so that here we only sketch the approach. The goal is to correctly describe the *asymptotic limit* of the final state broadening, which is defined by the approximations of very high Q and hard sphere short distance interactions between He atoms. Real experiments are sufficiently close to these conditions that the extension to finite Q and to the real He–He interactions should not introduce serious error. The results of many–body calculations (e.g. GFMC, PIMC, variational) of ground state properties, such as $n(p)$ and $g(r)$, should be used as inputs without recalculating them. Therefore, a projection superoperator method was chosen which enables a perturbation expansion for the dynamical response about the strongly interacting ground state. The final results, Eqs. (18–20), have been subsequently derived by Rinat and Butler [23] using a multiple scattering formalism which provides a more familiar derivation for some readers.

The projection approach relies on an exact relation between the neutron scattering law and a projection superoperator for single particle–hole excitations out of the true ground state. A Dyson equation can be derived by a Mori–Zwanzig–type [24] perturbative expansion of the Liouville equation for the time evolution of the single particle–hole excitations. All atom–atom scatterings are resummed to all orders in the interaction potential in terms of two–body *t*–matrices, and all interactions between three or more atoms are ignored. The "effective interaction" is then a product of a two–body *t*–matrix times the two–body density matrix in the ground state, which effectively screens the strongly repulsive short distance behavior resulting in a small parameter expansion. All terms which do not survive in the asymptotic limit are also ignored. Since Q is large, a semi–classical on–shell approximation [25] can be used for the two–body *t*–matrix. The two–body density matrix is approximated as a factorizable product of $n(p)$ and $g(r)$ in a way which satisfies the sum rules. The resulting Dyson equation may then be solved analytically.

A Feynman diagram representation of the resulting Dyson equation is shown in Fig. 6. The neutron scattering law describes the propagation of a particle–hole excitation above the ground state, which removes a particle of wave vector k and creates a particle of wave vector $k+Q$. Arrows denote the direction of the flow of momentum. A right arrow denotes a particle line and the left arrow a hole line. Only the particle lines can carry high momentum on the order of Q, whereas the hole lines must carry low momenta characteristic of the ground state wave function. The hatched area denotes the exact result including all scatterings of particles and holes. In the impulse approximation, the particle and hole are assumed to propagate without scattering. The final state effects come from the scattering of the high momentum particle creating new particle–hole excitations. The approximation indicated keeps only a single additional particle–hole excitation. The shaded box represents the two–particle density matrix describing the correlations between the two holes in the ground state, which is related by sum rules to the radial distribution function, $g(r)$. The dashed line is the two particle *t*–matrix which describes the scattering. The fact that the hatched area appears in both the exact result and the final state effects diagram im-

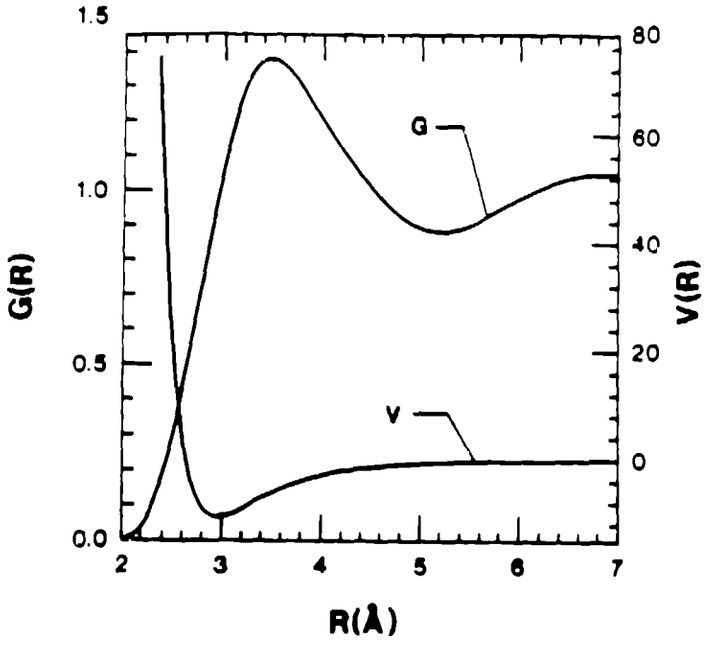

Fig. 5 Radial distribution function, $g(r)$, for liquid ^{4}He as measured by neutron diffraction, and the He–He potential, $V(r)$.

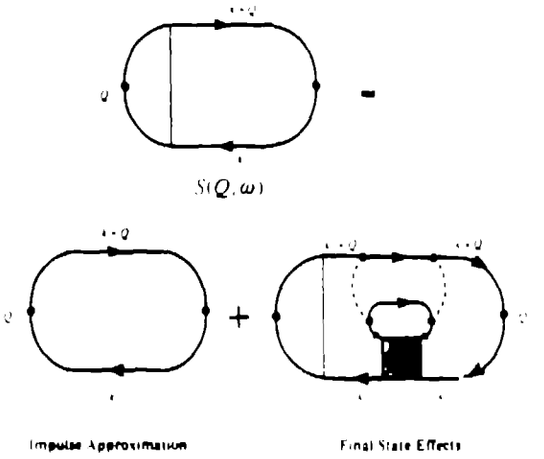

Fig. 6 Feynman diagram representation of the Dyson equation for deep inelastic neutron scattering. The left arrow denotes a hole line, the right arrow a particle line. The dashed line represents the He–He t–matrix. The box represents the two–particle density matrix in the ground state. The apperance of the hatched area on both sides of the equation indicates that the equation must be solved self–consistently.

plies that the scattering processes which transform a $(\kappa+Q,\kappa)$ excitation to a $(\kappa'+Q,\kappa')$ excitation must be calculated self–consistently.

The predicted final state broadening obtained again takes the form of an integral over a classical trajectory,

$$R_{FS}(Y,Q) = \frac{1}{2\pi}\int_{-\infty}^{\infty} dx\ \exp\left[iYx - \int_{0}^{|x|}\Gamma(x')dx'\right] \quad , \qquad (18)$$

which should be compared to Eq. (17). The collision rate per unit distance traveled is given by

$$\Gamma(x) = -\pi\rho\int_{0}^{\infty} db^2\ f_b\ g(\sqrt{x^2+b^2}) \quad , \qquad (19)$$

where b is the impact parameter for the collision. The quantity f_b can be written in terms of the scattering phase shifts, $\delta\ (b)$, as

$$f_b = e^{2i\delta(b)} - 1 + e^{2i\delta(b) - i\infty Qb/2} \quad . \qquad (20)$$

The $\delta(b)$ are calculated in the Jeffreys–Wentzel–Kramers–Brillouin (JWKB) approximation, which is valid at high Q no matter how steeply repulsive the potential. We note that $\Gamma(\infty) = \rho\ \sigma_{tot}(Q)/2$. The third term in Eq. (20) results in the glory oscillations of $\sigma_{tot}(Q)$. More generally, Eqs. (18–20) may be interpreted as the result of a WKB classical trajectory calculation of the final state broadening in which the quantity $\Sigma(x) \equiv -i\hbar^2 Q\Gamma(x)/2M$ serves as an *optical potential.*

PREDICTIONS FOR EXPERIMENT [26]

Figure 7 shows the final state broadening calculated for $Q = 30\ \text{A}^{-1}$ from Eqs. (18–20) using as input the experimental $g(r)$ obtained by neutron diffraction. One can see that the FWHM approximately obeys Eq. (12), but the broadening function goes negative at large $|Y|$ in order to satisfy the second moment sum rule. The final state broadening is not a narrow function, but rather it shifts $J(Y,Q)$ intensity among different Y regions. Figure 8 shows the integrand of the second moment sum rule over a larger range of Y. While the area under the curve is zero as required, the broadening function oscillates between positive and negative values at large $|Y|$, the scale of which is primarily controlled by the structure in $g(r)$ shown in Fig. 5.

Figure 9 shows the effect of the final state broadening on the measureable Compton profile for the normal fluid at $T = 3.3\ ^{\circ}\text{K}$ and $Q = 30\ \text{A}^{-1}$, using the Path Integral Monte Carlo (PIMC) momentum distribution [10] as input to the calculation. The dashed line is the impulse approximation prediction. The solid line (FS) is the prediction after including final state broadening. Final state effects are very small for the normal fluid. The calculated momentum distribution for the normal fluid is almost Gaussian, and the second moment sum rule requires that final state effects cannot alter the Gaussian width of the Compton profile. In contrast, the pluses in Fig. 9 shows the prediction of the Lorentzian broadening theory (LZ), Eq. (11).

Figure 10 shows the same comparison for the superfluid at $T = 0.0\ ^{\circ}\text{K}$, using as input the Green's Function Monte Carlo [9] momentum distribution. The dashed line is the impulse ap-

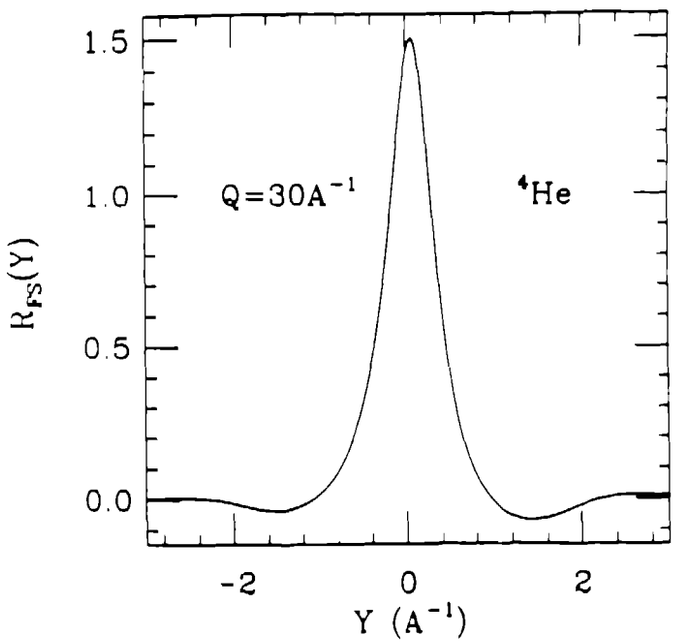

Fig. 7 Final state broadening function for ^{4}He, $R_{FS}(Y)$, predicted by Eqs. (18–20) at $Q = 30$ A^{-1}.

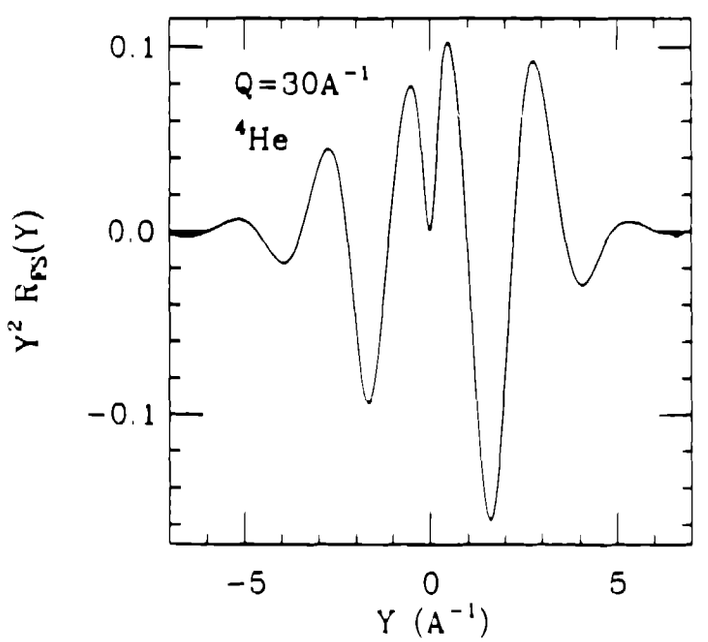

Fig. 8 A plot of $Y^2R_{FS}(Y)$ vs. Y for ^{4}He at $Q = 30$ A^{-1}. The area under this curve must be zero in order to satisfy the second moment ("kinetic energy") sum rule on the neutron scattering law.

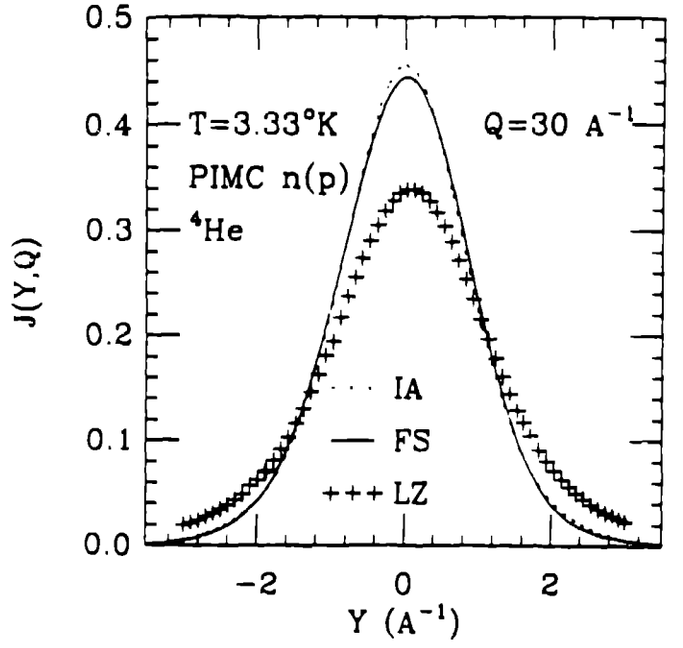

Fig. 9 Compton profiles, $J(Y,Q)$, predicted for normal liquid ^{4}He at $T = 3.33$ °K and $Q = 30$ A^{-1} using the PIMC momentum distribution. The dashed line is the prediction of the impulse approximation (IA). The solid line is the prediction of the final state effects theory (FS), Eqs. (18–20). The pluses represent the prediction of the Lorentzian broadening theory (LZ), Eq. (11).

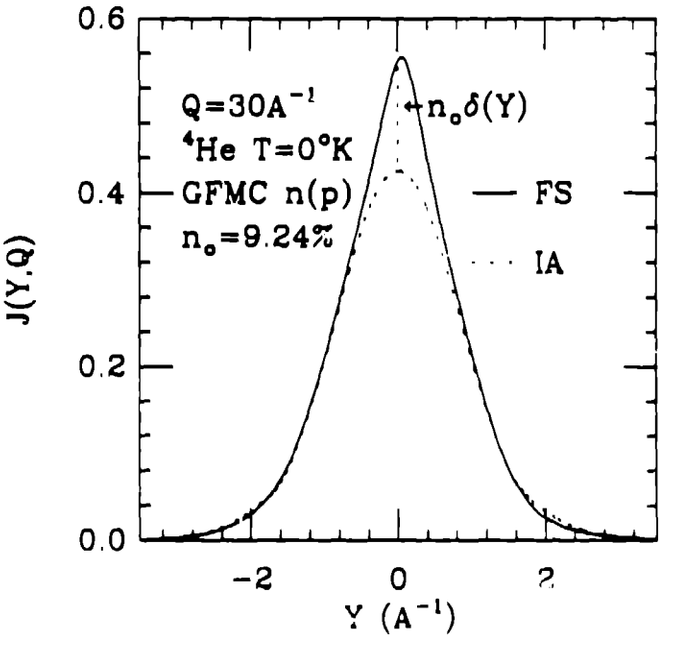

Fig. 10 Compton profiles predicted for superfluid ^{4}He at $T = 0$ °K and $Q = 30$ A^{-1} using the GFMC momentum distribution. The dashed line is the prediction of the impulse approximation (IA), and the solid line is the prediction of the final state effects theory (FS), Eqs. (18–20).

Bose condensate of weight 9.24 %. The solid line is the prediction after including final state broadening. Final state effects are much larger for the superfluid. The FWHM is scarcely changed in accordance with the second moment sum rule. But the Compton profile predicted for the superfluid is distinctly more sharply around $Y = 0$ than for the normal fluid. The Bose condensate no longer results a distinct peak sitting atop a broader background.

Figure 11 shows another way to view the results for the superfluid. The dashed line is the GFMC momentum distribution shown earlier. The solid line is the "apparent momentum distribution" which might be inferred from the final state broadened Compton profile shown in Fig. 10, obtained by analyzing the data using the impulse approximation expression, Eq. (6). This looks very similar to some earlier results on momentum distributions obtained from reactor data [11].

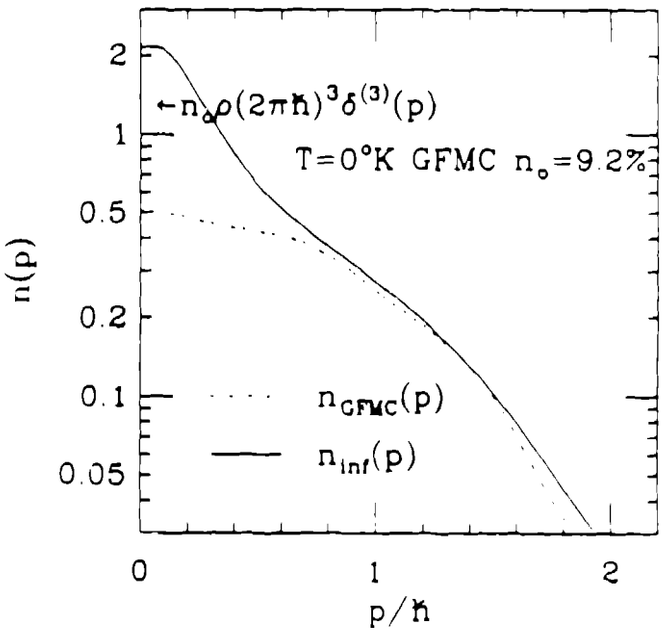

Fig. 11 The solid line is the apparent momentum distribution which would be obtained by analyzing final state broadened data, such as the solid line in Fig. 10, as if the impulse approximation was correct according to Eq. (6). The dashed line is the GFMC momentum distribution.

However, some words of caution are in order regarding comparing the results of Eqs. (18–20) directly to experiment.

First, the derivation has left out a large number of terms which vary as $O(Q^{-1})$ with increasing Q. While these are not important in the asymptotic limit, they may be of importance for the Q's achievable in real experiments. These include the initial self energy of the atom in the many–body state before the neutron collision, the off–shell behavior of the t–matrix, corrections to the semiclassical approximation, etc. For example, the semiclassical methods begin to perceptibly fail at $Q < 10$ A^{-1}. Eqs. (18–20) may be fairly accurate for the high Q's achievable at pulsed neutron sources. They may require significant corrections in order to describe reactor experiments at $Q < 10$ A^{-1}. The asymmetry in the lineshapes observed at low Q's is not contained within Eqs. (18–20). The apparent width oscillations observed at low Q's are not predicted by Eqs. (18–20).

responsible for glory oscillations of the He–He total cross section.

Second, the convolution form of the final state broadening depends on the approximation used for the two–body density matrix as a factorizable product of $n(p)$ and $g(r)$. Ristig and Clark [27] have pointed out that this choice does not satisfy a number of other known properties of the two–body density matrix. The convolution form, Eq. (10), does not hold when a more correct two–body density matrix is used as input. Clark and Ristig have recently calculated two–body density matrices for ^{4}He using a Jastrow ansatz, and they have deduced the general structural form for the two–body density matrix for any wave function. These should be used in a more accurate calculation of the scattering law. Even if the quantitative changes turn out to be small, such a calculation is conceptually important in view of the classical trajectory interpretation of the Y–variable discussed earlier.

Nevertheless, the semi–quantitative predictions of Eqs. (18–20) should be valid for $Q > 10$ A^{-1}, and the Dyson equation represented by Fig. 6 should form the basis for more precise calculations of final state effects for momentum distribution experiments by deep inelastic scattering.

EXPERIMENTAL RESULTS

A new set of deep inelastic experiments [8,28,29] on liquid ^{4}He have been performed at the Intense Pulsed Neutron Source at the Argonne National Laboratory by a team led by P. Sokol and which included T. R. Sosnick, W. M. Snow, and K. Herwig. The experiments were performed on the PHOENIX chopper spectrometer, which was designed as a dedicated instrument for deep inelastic scattering experiments. Compared with the earlier low Q reactor experiments, the new experiments used the very high epithermal neutron flux of the pulsed source to reach much higher Q's, and they also had a much better characterization of the instrument resolution function which is essential to accurate lineshape studies. Compared with earlier measurements at comparable or higher Q's, the new experiments are the first to have sufficient instrumental resolution to reliably extract the lineshape.

The data analysis avoided the model fitting procedure with n_0 as a free parameter which has been attempted with reactor data taken up to 1982. Instead, experiment and *ab initio* theory were directly compared without any adjustable parameters. The theory is obtained by combining the new accurate many–body calculations of momentum distributions published in 1984–87 and the theory for final state effects [21,22] first presented in 1987. It is essential to recognize that the data are further broadened by the instrument resolution function, which should be convoluted with the theoretical predictions for the Compton profile. The spectrometer resolution function is calculated by a Monte Carlo simulation. At $Q = 23$ A^{-1}, the FWHM of the instrumental broadening is comparable to that of the final state broadening predicted by Eqs. (18–20). There was also an absolute intensity calibration of the data within 5 %. Details of the instrument and how the raw data were processed to extract the Compton profiles are discussed in ref. [28].

The data [8] in Fig. 12 were taken at $Q = 23$ A^{-1} in the normal fluid at $T = 3.5$ °K. The data in Figure 13 were taken at $Q = 23$ A^{-1} in the superfluid at $T = 0.35$ °K. One can see that the data are somewhat more sharply peaked around $Y = 0$ in the superfluid, as expected if a Bose condensate were to form. The dashed line in Fig. 11 is the PIMC–IA prediction of Fig. 8, convoluted with the instrumental resolution function. The solid line is obtained after further convoluting with final state effects. One can see that the normal fluid data are in excellent agreement with both the im-

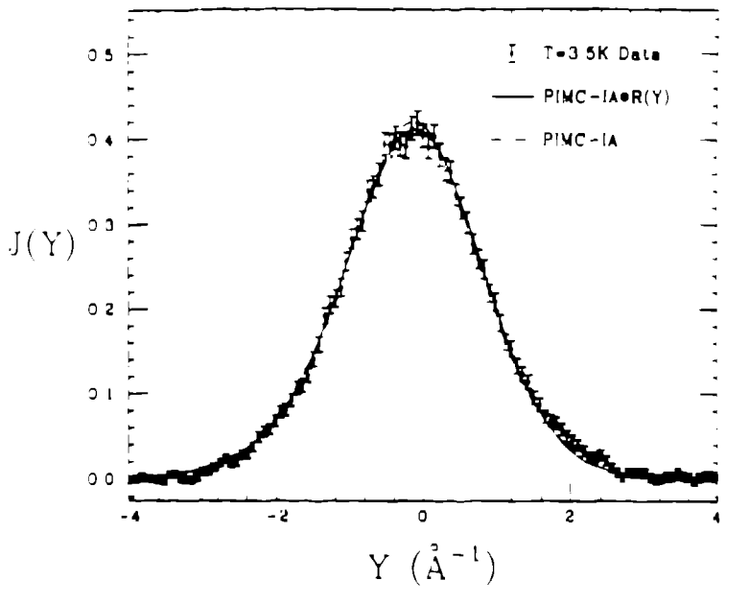

Fig. 12 The data is the measured Compton profile in normal liquid ^{4}He at $T = 3.5$ °K and $Q = 23$ Å^{-1}. The dashed line is the prediction of the PIMC momentum distribution and the impulse approximation, broadened by the instrumental resolution function. The solid line is the prediction after further broadening by the final state effects function shown in Fig. 7.

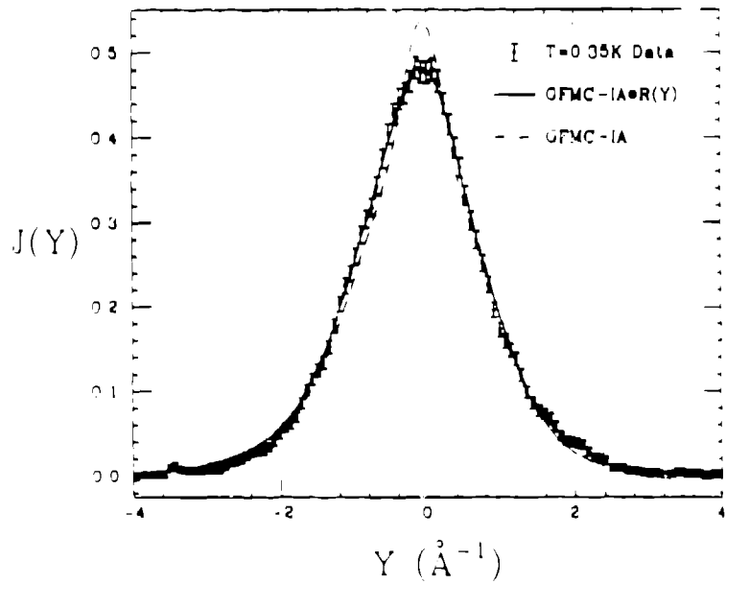

Fig. 13 The data is the measured Compton profile for superfluid liquid ^{4}He at $T = 0.35$ °K and $Q = 23$ Å^{-1}. The dashed line is the prediction of the GFMC momentum distribution and the impulse approximation, broadened by the instrumental resolution function. The solid line is the prediction after further broadening by the final state effects function shown in Fig. 7.

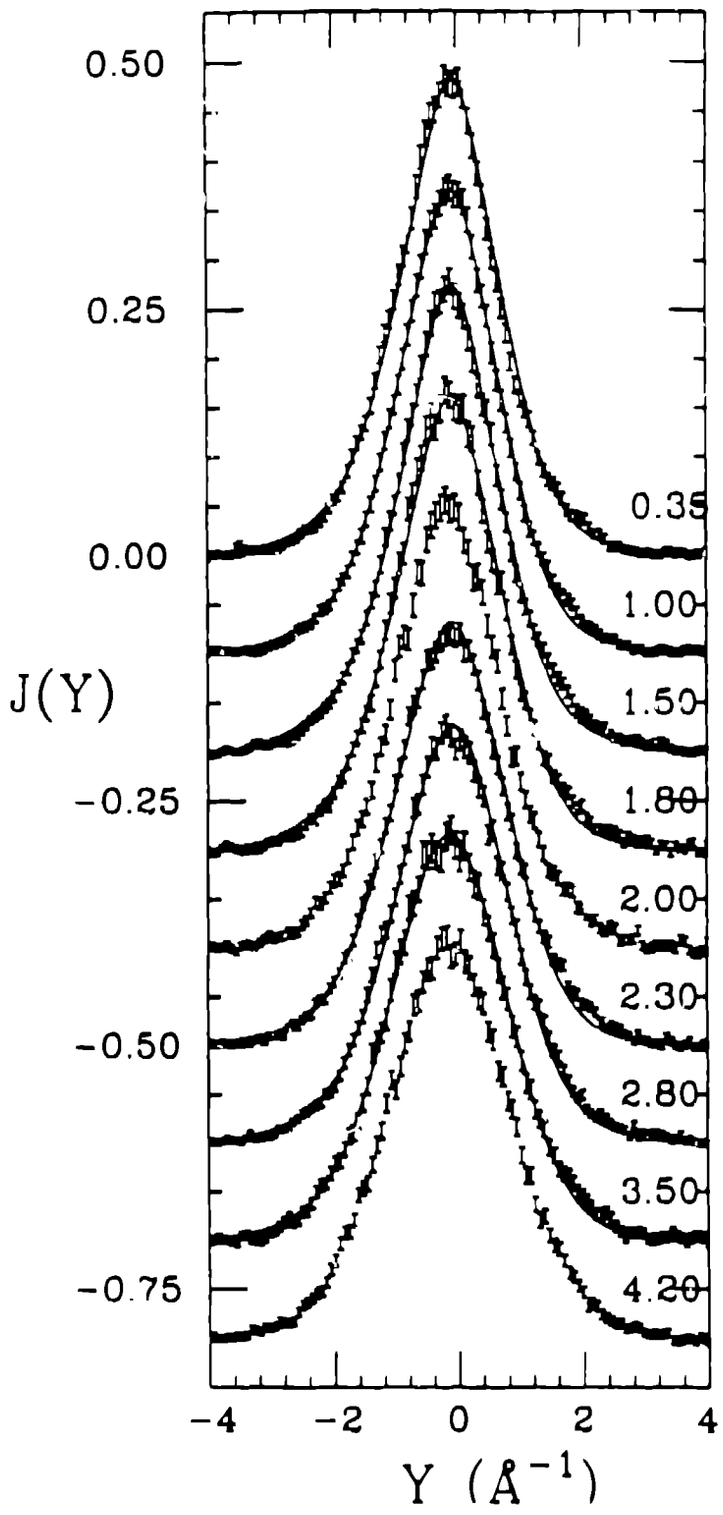

Fig. 14 Observed scattering at temperatures of 0.35, 1.0, 1.5, 1.8, 2.0, 2.3, 2.8, 3.5 and 4.2 °K. The solid lines a e the theoretical predictions with instrumental resolution and final state effects included. GFMC calculations are used for comparison with the 0.35 °K results. PIMC calculations are used for the remainder of the temperatures. No calculations are available for comparison with the 2.0 and 4.2 °K measurements.

data disagree with Lorentzian broadening curve shown in Fig. 9 and given by Eq. (11). For the superfluid data in Fig. 12, the dashed line is again the GFMC–IA prediction of Fig. 10 again convoluted with the instrumental broadening, and the solid line is the result obtained after further broadening with final state effects. The superfluid data disagree with the impulse approximation, but they are in excellent agreement with the GFMC–IA theory broadened by final state effects.

Thus, *ab initio* theory and experiment are in excellent agreement for both the normal fluid and the superfluid with no adjustable parameters, and they are consistent with a Bose condensate fraction in the superfluid of 9.24% at $T = 0$ °K! Experiment and ab initio theory are in fact consistent for all temperatures measured, as shown in Fig. 14.

One may wonder about the importance of the condensate induced small–p singularities which played a significant role in the data analysis of the reactor experiments. Clearly the GFMC momentum distribution shown in Fig. 2 does not show these singularities, presumably because of the finite system size which can be simulated in a feasible Quantum Monte Carlo calculation. However, a variational Hypernetted Chain calculation [30] which correctly includes these singularities is also in excellent agreement with the superfluid data, and it predicts almost the same Compton profile as GFMC. The reason the singularities have a relatively small effect is that in Eq. (6) $n^*(p)$ is multiplied by p. This suppresses the contribution of the p^{-1} term in Eq. (7). However, a singular term varying as, say, p^{-4} would still result in strongly singular behavior in $J_{IA}(Y)$. Thus, the Bose condensate which is infinitely singular still shows up strongly in $J_{IA}(Y)$, even though the predicted [14] small–p singular terms do not. More generally, the inference of the low p part of $n^*(p)$ from the Compton profile data is an extremely ill–posed problem [3,28,31] in the presence of statistical error.

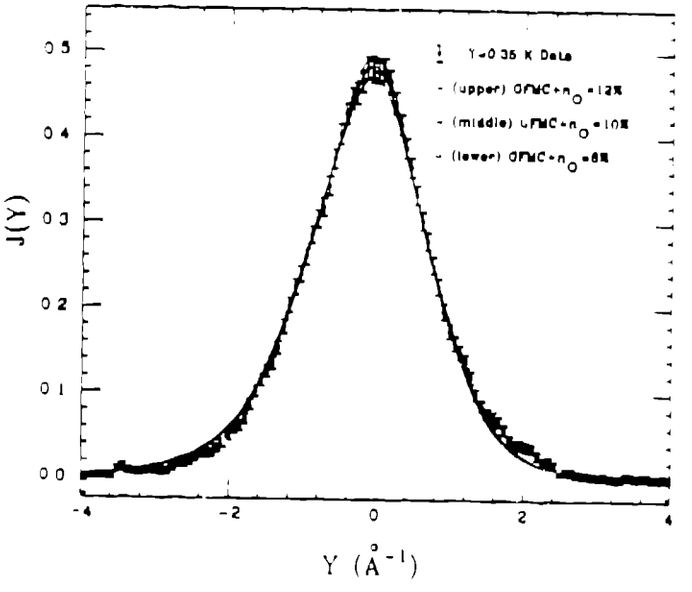

Fig. 15 Sensitivity of the observed scattering to the magnitude of the condensate fraction at $T = 0.35$ °K. GFMC calculations have been used for the uncondensed component, and a narrow Gaussian to represent the condensate. The best agreement is obtained for $n_0 = 10$ %. The two limiting values, $n_0 = 8$ and 12 %, are the lower and upper lines respectively.

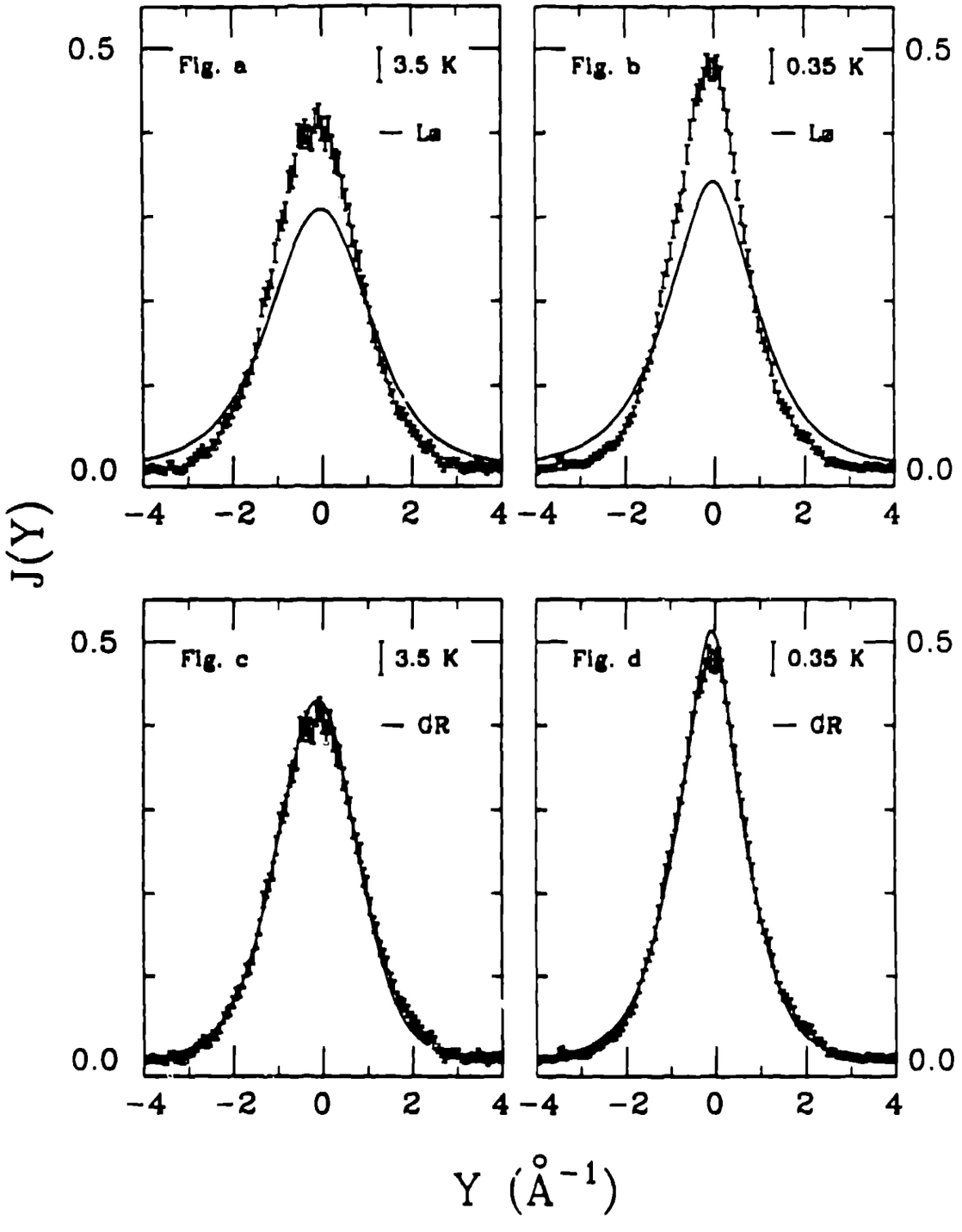

Fig. 16 Comparison of the normal and superfluid data at $Q = 23$ Å^{-1} with other theories for final state effects: the lines in a) & b) are the predictions of the 1966 Lorentzian broadening theory (LZ), Eq. (11); the lines in c) & d) are the predictions of the 1973 theory of Gersch and Rodriguez (GR).

One can ask how sensitive the experiment is to the actual value of the Bose condensate fraction. Fig. 15 shows the effect of changing the condensate fraction to 8 and 12 %, from the best fit value of 10 %, assuming GFMC for the non–condensed atoms and the final state broadening theory. Application of the model fitting procedure [12] to these new high Q data would yield a Bose condensate around 9 %, provided that the low–p singularities are treated correctly [15] and that corrections due to final state effects are added to the procedure. A more complete discussion is presented in ref. [28].

Assuming that the momentum distribution calculations are correct, one can use these data to test the other theories for final state broadening [32]. Figure 16 (a & b) shows the comparison of the data with the Lorentzian broadening prediction [33] obtained by taking the limit of a structureless fluid, i.e. $g(r) \rightarrow 1.0$ in Eqs. (18–20). The disagreement is strong for both the normal and the superfluid. Figure 16 (c & d) shows the comparison with the original theory of Gersch and Rodriguez [17,18,34]. The final state broadening is qualitatively correct, but it is quantitatively too small compared to the data. However, considering the necessary crudeness of the approximations made (eikonal approximation for the t–matrix, step function approximation for $g(r)$, etc.) at the time, the agreement between the Gersch and Rodriguez 1973 theory and the latest 1989 experiment is impressive.

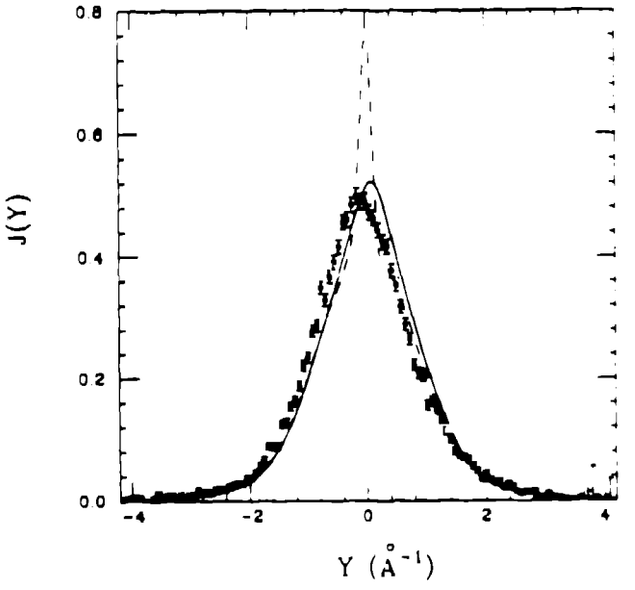

Fig. 17 Preliminary data for the superfluid at $Q = 13$ Å^{-1} and $T = 0.7$ °K. The dashed line is the prediction of the impulse approximation using the GFMC momentum distribution and broadened by the instrumental resolution function. The solid line is the prediction after further broadening by the final state effects predicted by Eqs. (18–20). See the text.

Recently new experiments [29] have been performed at lower Q's for which the instrumental resolution is much smaller than the final state broadening. Figure 17 shows preliminary data for the superfluid at $T = 0.7$ °K and $Q = 13$ Å^{-1}. Again the dashed line is the GFMC–IA prediction at $T = 0.0$ °K convoluted with the (much narrower) instrumental resolution function at

[illegible] of the Bose condensate is much sharper than the data. The solid line shows the prediction after including final state broadening. Now, the peak shape and height are in excellent agreement with experiment.

However, there is a shift in the data to negative Y compared with theory by about one channel, approximately 0.07 A^{-1}. The origin of this discrepancy is unclear. A simple argument [35] suggests that this shift is inconsistent with f– and second moment sum rules on $S(Q,\omega)$ by more than nine standard deviations. A similar shift of the same magnitude is seen at $Q = 18$ A^{-1} and at a variety of temperatures, and indeed the original data at $Q = 23$ A^{-1} were also shifted by the same amount. If the Y–scale were shifted by the small amount required to satisfy the f–sum rule, the agreement between the final state broadened GFMC–IA theory and experiment would again be excellent, presenting an even more convincing case for the final state effects theory in view of the superior instrumental resolution at these lower Q's. However, the correct calibration of the Y–scale should ultimately be resolved by the experimentalists.

IMPLICATIONS FOR FUTURE MOMENTUM DISTRIBUTION STUDIES

Despite the few uncertainties discussed in the previous sections, one must conclude that *ab initio* many–body theory, the theory of final state effects, and neutron scattering experiment have all converged for deep inelastic neutron scattering on liquid ^{4}He. Although a sharp peak in the scattering law due to a Bose condensate appears to be unobservable by deep inelastic scattering, experiment and theory are consistent with a Bose condensate fraction in the superfluid of 9.2 % at zero temperature. In this section, we discuss the implications of this achievement for future deep inelastic scattering studies.

First, there remains much to do on liquid ^{4}He. An analysis of the existing extensive data at very low Q ($\leq$ 10 A^{-1}) may require significant additonal inputs to the final state effects theory for the many $O(Q^{-1})$ effects which have been left out in the asymptotic limit of high Q and hard sphere interactions. In the currently accessible Q range (< 30 A^{-1}), higher accuracy and lower background measurements may begin to reveal the two–body density matrix effects which have been discussed by Clark and Ristig [27]. These include possible deviations from the convolution form of the final state broadening. Most importantly, higher Q and higher resolution experiments on ^{4}He are needed to further test and refine the theory of final state effects. Figure 18 shows the predictions in the region near $Y = 0$ for superfluid ^{4}He for much larger Q's. Even at the experimentally unfeasible value of $Q = 270$ A^{-1} no distinct condensate peak is predicted in $J(Y,Q)$. These predictions depend on the He–He potential at short distances [36] which has been calculated, but has not been adequately measured, by atom–atom scattering experiments. However, since higher Q experiments require a percentage energy resolution which varies as $O(Q^{-1})$, they may be extremely difficult to perform. There is also great interest in experiments aimed at measuring the Bose condensate fraction for ^{4}He in other physical conditions such as in 2–dimensional films, in disordered media, ^{3}He/^{4}He mixtures, etc. Presumably the final state effects theory discussed here can be adapted with minimal changes to describe these situations.

The atomic system of most interest to study next will be normal liquid ^{3}He, because of the controversy about the existence of a sharp Fermi surface discontinuity in the momentum distribution, as shown in Fig. 19. A non–interacting (*ideal*) gas of Fermions would have a discontinuity of 1.0, several many–body calculations for real ^{3}He [37,38] predict a discontinuity of approximately 0.3, and novel alternative wave functions have been proposed [39] which predict a Fermi surface discontinuity is 0.0. In the impulse approximation the effect of a Fermi surface disconti-

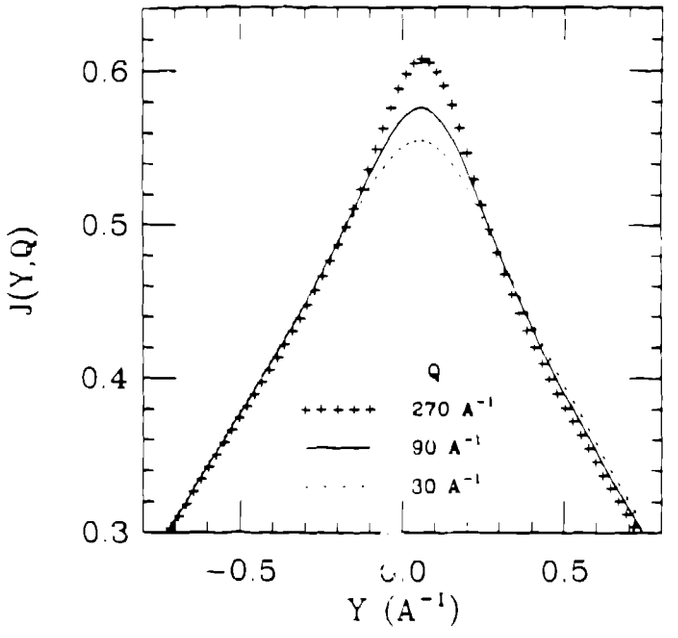

Fig. 18 Compton profiles with increasing Q for superfluid ^{4}He at $T = 0$ °K predicted by the final state effects theory. Only the region near $Y = 0$ A^{-1} relevant to the Bose condensate is shown. The condensate does not result in a distinct peak at any experimentally feasible Q.

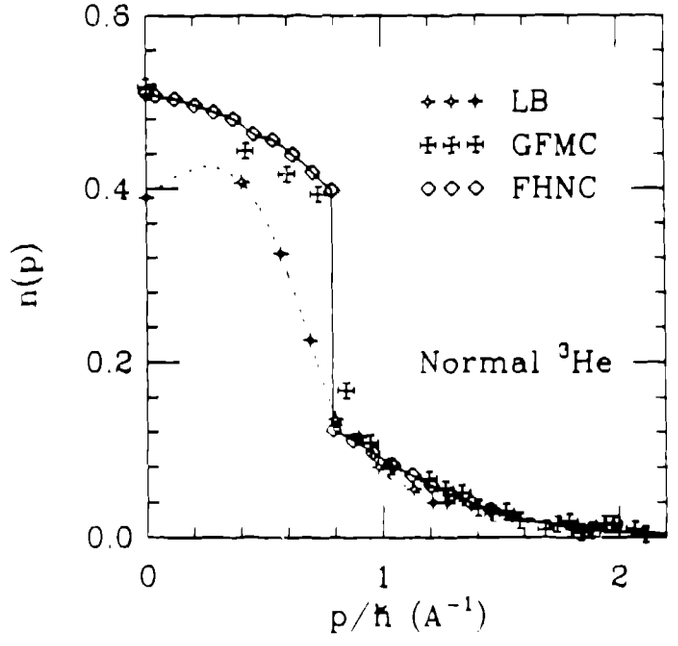

Fig. 19 Theoretical momentum distributions for normal liquid ^{3}He. The diamonds represent the Fermi Hypernetted Chain (FHNC) prediction with Fermi surface discontinuity at $p_F = 0.789$ A^{-1}. The crosses represent the Green's Function Monte Carlo (GFMC) result. The small crosses represent the prediction of the BCS pairing theory of Lhuillier and Bouchaud (LB) which lacks a Fermi surface discontinuity.

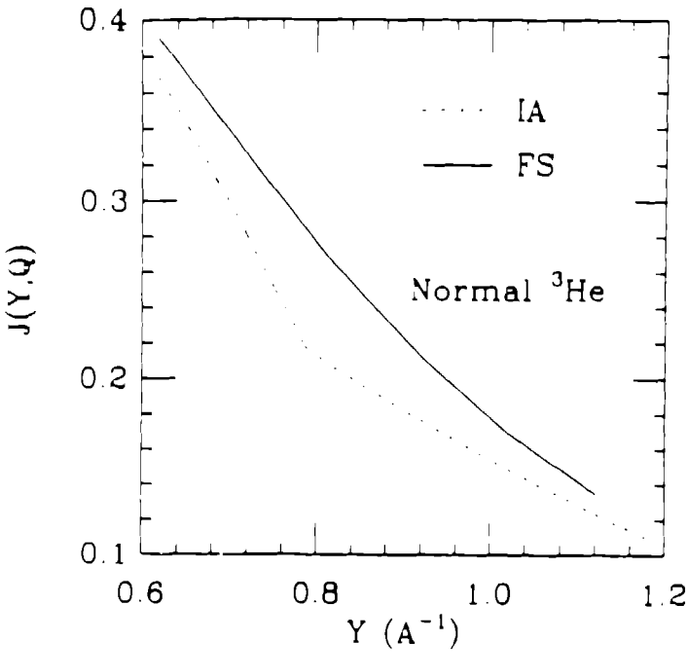

Fig. 20 Part of the Compton profile for normal liquid ^{3}He in the region near $Y = p_F/\hbar$. The dashed line is the impulse approximation (IA) prediction using the FHNC momentum distribution, showing a change in slope at $Y = p_F/\hbar$. The solid line (FS) is the prediction after broadening by final state effects, in which the discontinuity in slope is smoothed out.

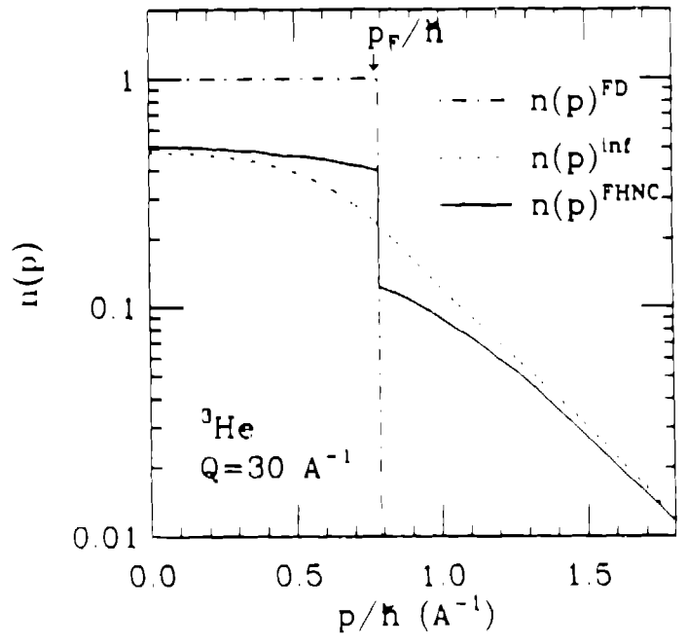

Fig. 21 Comparison of momentum distributions for ^{3}He. The curve labeled $n(p)^{FD}$ is the Fermi–Dirac distribution for a non–interacting gas at the same density, with discontinuity of 1.0 at the Fermi surface. The curve labeled $n(p)^{FHNC}$ is the Fermi Hypernetted Chain (FHNC) prediction with discontinuity of 0.3. The dashed line, $n(p)^*$ is the apparent momentum distribution which would be obtained by analyzing final state broadened data as if the impulse approximation were correct.

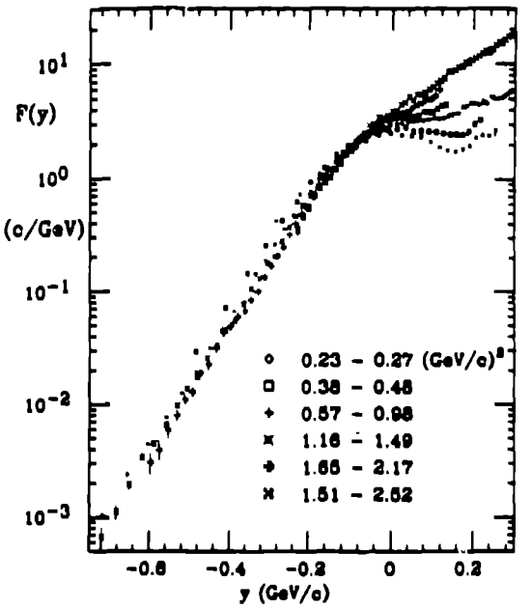

Fig. 22 Quasielastic electron nucleus scattering (QENS) from ^{12}C at several different relativistic 4–momentum transfers. For $-Y > 0.1$ GeV/c the results all fall on the same curve, illustrating the Y–scaling behavior. Y–scaling breaks down for larger values of Y due to the excitation of internal degrees of freedom of the nucleon.

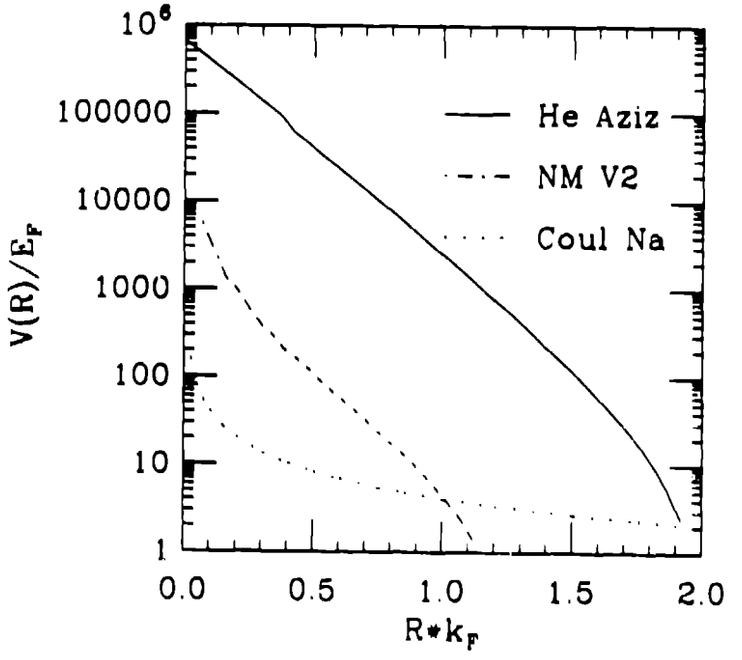

Fig. 23 Comparison of repulsive cores of the interaction potentials for atomic, electronic and nuclear systems. The potentials are scaled by the Fermi energy, E_F, and the distances are multiplied by the Fermi wave vector, k_F. The solid line is the ^{3}He Aziz potential, the long dashed line is the nuclear matter v_2 potential, and the short dashed line is the Coulomb potential for Na.

Compton profile is a change in slope at Y equal to the Fermi wave vector, k_F = 0.789 A^{-1}. The predictions for the Compton profile for Y near k_F are shown in Fig. 20. With the inclusion of final state broadening, even this change in slope is predicted to be smoothed over. In Fig. 21 the apparent momentum distribution for ^{3}He is displayed in an analogous fashion to Fig. 11 for ^{4}He. The apparent Fermi surface obtained by analyzing the final state broadened Compton profile assuming the impulse approximation relation, Eq. (6), is unobservable due to final state effects. Nevertheless, as was the case for the "unobservable" Bose condensate peak in ^{4}He, one should still be able to test the *ab initio* many body calculations for ^{3}He by deep inelastic scattering experiments. Such experiments are a formidable undertaking because of the additional complication of the very strong neutron absorption in ^{3}He.

Finally, we turn to quasielastic electron nucleus scattering [40,41]. In this case, the term "quasi–elastic" refers to the absence of change in the rest mass of the nucleon in the scattering process, even though the energy and momenta transferred are large compared to the energies characterizing collective behavior. The term "deep–inelastic" is reserved for experiments which probe the quark substructure of the nucleon. Despite this unfortunate semantic confusion, the physics is the same as for neutron scattering from He: i.e. the energies and momenta transferred by the electron are much larger than the binding energies of nucleons inside nuclei. Figure 22 shows a Y–scaling plot for electron scattering from the ^{12}C nucleus, where the relativistic 4–momentum range for each data set is shown and the Y–variable has been generalized to relativistic kinematics. This is meant to be analogous to Fig. 1 for deep inelastic neutron scattering from ^{4}He. Figure 22 shows that the Y–scaling is observed for negative Y, but that *Y–scaling is broken* for positive Y because of the possibility of exciting internal degrees of freedom such as the Δ (1238 MeV) resonance. The critical question is whether the impulse approximation can be applied to extract the momentum distribution from these data, and in particular whether the quasi–exponential dependence of the Compton profile on Y observed over four orders of magnitude reflects a quasi–exponential dependence of the nucleon $n(p)$ in nuclei.

To understand the possible importance of final state effects in this problem, we consider a comparative plot of the nucleon–nucleon potential [42], the He–He potential [36], and the Coulomb potential for Na shown in Fig. 23. The potentials are scaled by the Fermi energy and the distances are scaled by the Fermi momentum. The Coulomb potential is the softest at short distances, which is the reason that final state effects are relatively unimportant for x–ray Compton scattering experiments on electron momentum distributions. The nucleon–nucleon potential is much more steeply repulsive at short distances, and the He–He potential is several orders of magnitude harder than that. Thus, we expect that the impulse approximation will be approached more quickly with increasing Q for nuclear physics than for He. However, kinematics requires that Q and ω should be low enough to avoid excitation of internal degrees of freedom of the nucleon. Comparatively, while neutron scattering on ^{3}He can reach Q/k_F of more than fifty, quasielastic electron nucleus scattering is restricted to Q/k_F less than ten. The combination of these two effects leads to the expectation that final state effects should be as important for quasielastic electron nucleus scattering as they are in deep inelastic neutron scattering from He.

Detailed calculations for quasielastic electron nucleus scattering have not yet been carried out [6]. They suffer from uncertainties regarding the appropriate choice of nuclear potential. They potentially require inclusion of all the $O(Q^{-1})$ effects which were left out of the asymptotic theory for neutron scattering from He. And the relativistic effects are a further essential complication. Nevertheless, we expect that the leading term of the theory to be represented by the same Dyson equation shown in Fig. 6.

ACKNOWLEDGEMENTS

Richard N. Silver is supported by the U. S. Department of Energy under Office of Basic Energy Sciences / Division of Materials Science (OBE3/DMS) support of the Manuel Lujan Jr. Neutron Scattering Center (LANSCE). Paul E. Sokol is supported by NSF Grant DMR–8704288 and OBES/DMS support of the Intense Pulsed Neutron Source at Argonne National Laboratory. We thank our colleagues whose work we report here, in particular T. R. Sosnick, W. M. Snow, and K. Herwig. We also thank J. W. Clark for earlier collaborations on much of this work.

REFERENCES

[1] F. London, Nature **141**, 643 (1938).

[2] For a tutorial discussion of the relation beween Bose condensation and superfluidity see D. R. Tilley, J. Tilley, *Superfluidity and Superconductivity*--2nd edition, Adam Hilger Ltd., 1986.

[3] For a complete review of the current state of the art, see *Momentum Distributions*, R. N. Silver, P. E. Sokol, eds., Plenum Press, 1989. For an introductory survey of momentum distribution studies across all of physics, see the article by P. E. Sokol, R. N. Silver, J. W. Clark, p. 1–38.

[4] P. C. Hohenberg, P. M. Platzman, Phys. Rev. **152**, 198 (1966); see also A. Miller, D. Pines, P. Nozieres, Phys. Rev. **127**, 1452 (1962).

[5] G. B. West, Physics Reports **18C**, 263 (1975); see also G. B. West, in ref. [3], p. 95–110.

[6] J. W. Clark, R. N. Silver, *Proceedings of the Third International Conference on Nuclear Reaction Mechanisms*, Varenna, Italy, June 13–18, 1988, E. Gadioli, ed. (Ricerca Scientifica ed Educazione Permanente, Universita degli Studi di Milano), Supplemento 66, p. 531–540 (1988).

[7] W. G. Stirling, E. F. Talbot, B. Tanatar, H. R. Glyde, J. Low Temperature Physics, **73**, 33 (1988)

[8] T. R. Sosnick, W. M. Snow, P. E. Sokol, R. N. Silver, Europhysics Letters **9**, 707 (1989).

[9] P. Whitlock, R. M. Panoff, Can. J. Phys. **65**, 1409 (1987).

[10] D. M. Ceperley, E. L. Pollock, Can. J. Phys. **65**, 1416 (1987); see also D. M. Ceperley, in ref. [3], p. 71–80.

[11] For reviews, see H. R. Glyde, E. C. Svensson, in Methods of Experimental Physics, V. **23B**, D. L. Price, K. Skold, eds., Academic Press, 1987, p. 303–404; E. C. Svensson, V. F. Sears, Physica **137B**, 126–140 (1986).

[12] V. F. Sears, E. C. Svensson, P. Martel, A. D. B. Woods, Phys. Rev. Lett. **49**, 279 (1982).

[13] P. Martel, E. C. Svensson, A. D. B. Woods, V. F. Sears, R. A. Cowley, J. Low Temp. Phys. **23**, 285 (1976).

[14] J. Gavoret, P. Nozieres, Ann. Phys. (N.Y.) **28**, 349 (1964); P. C. Hohenberg, P. C. Martin, Ann. Phys. (N. Y.) **34**, 291 (1965).

[15] A. Griffin, Phys. Rev. **B32**, 3289 (1985).

[16] R. K. B. Helbing, J. Chem. Phys. **50**, 493 (1969).

[17] H. A. Gersch, L. J. Rodriguez, Phys. Rev. **A8**, 905 (1973).

[18] L. J. Rodriguez, H. A. Gersch, H. A. Mook, Phys. Rev. **A9**, 2085 (1974).

[19] P. Martel, E. C. Svensson, A. D. B. Woods, V. F. Sears, R. A. Cowley, J. Low Temp. Phys. **23**, 285 (1986).

[20] See also H. R. Glyde, W. G. Stirling, in ref [3], p. 111–122.

[21] R. N. Silver in *Condensed Matter Theories* , J. S. Arponen, R. F. Bishop, M. Manninen,

[22] [illegible] The latter paper contains a rather complete list of theoretical papers on final state effects in deep inelastic neutron scattering.
[23] A. Rinat, M. Butler, to be published.
[24] R. W. Zwanzig, Physica (Utrecht) **30**, 1109 (1964); see also P. N. Argyres, J. L. Sigel, Phys. Rev. Letts. **31**, 1397 (1973); Phys. Rev. **B9**, 3197 (1974).
[25] R. K. B. Helbing, J. Chem. Phys. **50**, 493 (1969).
[26] R. N. Silver, Phys. Rev. **B39**, 4022 (1989).
[27] M. L. Ristig, J. W. Clark, in ref. [3], p. 365–370; M. L. Ristig, J. W. Clark, Phys. Rev. **B40**, 4355 (1989).
[28] P. E. Sokol, T. R. Sosnick, W. M. Snow, in ref. [3], p. 139–158.
[29] K. Herwig, W. M. Snow, P. E. Sokol, to be published.
[30] E. Manousakis, V. R. Pandharipande, Q. N. Usmani, Phys. Rev. **B31**, 7022 (1985); E. Manousakis, V. R. Pandharipande, ibid., 7029; see also, E. Manousakis, in ref. [3], 81–94.
[31] D. S. Sivia, R. N. Silver, in ref. [3], p. 377–380.
[32] P. E. Sokol, R. N. Silver, T. R. Sosnick, W. M. Snow, in ref. [3], 385–392; W. M. Snow, T. R. Sosnick, P. E. Sokol, R. N. Silver, to be published.
[33] This is essentially the same as P. M. Platzman, N. Tzoar, Phys. Rev. **B30**, 6397 (1984).
[34] We thank Prof. Gersch for coming out of retirement to perform these calculations.
[35] R. N. Silver, to be published.
[36] R. Feltgen, H. Kirst, K. A. Koehler, F. Torello, J. Chem. Phys. **26**, 2360 (1982).
[37] P. Whitlock, R. M. Panoff, Can. J. Phys. **65**, 1409 (1987); see also R. M. Panoff, P. A. Whitlock, in ref. [3], p. 59–70.
[38] E. Manousakis, S. Fantoni, V. R. Pandharipande, Phys. Rev. **B28**,3370 (1983).
[39] J. P. Bouchaud, C. Lhuillier, Europhys. Lett. **3**, 1273 (1987); J. P. Bouchaud, C. Lhuillier, Z. Phys. **B75**, 283 (1989).
[40] For an experimental review, see I. Sick, in ref. [3], p. 175–186; D. Day, in ref. [3], p. 319–332.
[41] For a theoretical discussion, see O. Benhar, A. Fabrocini, S. Fantoni, in ref. [3], p. 187–202.
[42] V. R. Pandharipande, R. B. Wiringa, B. D. Day, Phys. Lett. **57B**, 205 (1975).